NICST Internal Memo

Date: September 8, 2010
From: J. McIntire
To: Bruce Guenther, Jim Butler, and Jack Xiong
Subject: Polarization Dependence of Optical Crosstalk from VIIRS F1 ETP-654, ETP-655, and ETP-663

References:

[1] ETP-663_VISNIR_FSF_v9, 'VISNIR Filter Spread Function (FSF) Test,' J. Parrilla and A. Choi.
[2] ETP-655_VISNIR_FSF_v4, 'VISNIR Filter Spread Function (FSF) during FP-16 part 1,' J. Parrilla and A. Choi.
[3] ETP-654_SpMA_RSO_v2, 'SpMA Polarized RSO Characterization,' J. Parrilla.
[4] NICST_REPORT_09_019, 'FU1 ETP-663: Preliminary Analysis,' J. McIntire, May 5, 2009.
[5] NICST_REPORT_09_094, 'Preliminary Analysis of ETP-655: Senders M1 and M4,' J. McIntire, July 31, 2009.
[6] NICST_REPORT_09_122, 'Preliminary Analysis of ETP-655,' J. McIntire, September 15, 2009.
[7] 'Polarization Dependent Crosstalk Update ETP-654/ETP-663,' Mau-song Chou, June 4, 2009.
[8] NICST_MEMO_10_017, 'Updated Analysis of VIIRS VisNIR Relative Spectral Response,' T. Schwarting, J. McIntire, and C. Pan, June 21, 2010.
[9] NICST_MEMO_10_022, 'Polarization Sensitivity Analysis for VIIRS F1 VisNIR Bands,' J. Sun, August 10, 2010.
[10] NICST_MEMO_10_018, 'VIIRS F1 FP-16 Part 2 band to Point Static Electrical Crosstalk from the Cold Focal Planes,' J. McIntire, June 23, 2010.
[11] NICST_REPORT_09_017, 'Summary of VIIRS FU1 ETP635 Data Analysis,' C. Pan, N. Che, and J. McIntire, May 1, 2009.
[12] NICST_MEMO_10_010, 'Summary of F1 Radiometric Calibration Performance for RSB from TV RC-02 Tests,' J. Sun and N. Che, May 3, 2010.
[13] NICST_MEMO_10_016, 'SIS100 Red Leak Investigation for VisNIR Bands,' J. McIntire, A. Tolea, and N. Che, June 14, 2010.
[14] NICST_REPORT_09_132,'NICST Crosstalk Methodology for FP-16 Crosstalk Map version 3.0,' T. Schwarting, November 11, 2009.

1. Introduction

The polarization dependence of optical crosstalk was investigated during the pre-TV test ETP-663 and the TV test ETP-655 [1,2]; the polarization dependence of the source was measured during ETP-654 [3]. The testing was confined to bands in the VisNIR focal plane. Testing was conducted in diagnostic mode with the telescope fixed. The test data used here is listed in Table 1. Preliminary analysis of the polarization dependence has been reported [4,5,6].

The Spectral Measurement Assembly (SpMA), a double monochrometer operating in subtractive mode, was used as the source for ETP-654, ETP-655, and ETP-663. Vertical slit and cross-slit configurations were used. The vertical slit configuration was aligned such that only a single band was illuminated at a time. The cross-slit configuration used a second vertical slit reticle, positioned perpendicular to the first vertical slit, such that only a single detector was illuminated at a time.

The SpMA is set to output at series of discrete wavelengths that correspond to tall poles in the OOB response; these wavelengths are given in Table 1. The tall poles were determined using data from STR-443 and transmission data taken by V. Murgai [7]. In addition, the SpMA is also set to the specified band center wavelength for each sender band.

A Wire Grid Polarizer (WGP) was placed in the optical path between the SpMA and the thermal vacuum chamber window. This polarizer was rotated during the test to isolate four polarization angles: 0, 45, 90, and 135 degrees.

2. ETP-654

Measurements of the SpMA Relative Spectral Output (RSO) were made with tungsten bulbs # 1 and #4 (see [8]). The SpMA output is partially polarized. The partially polarized RSO for both bulbs is shown in Figure 1 (both normalized to the maximum). For the purposes of this work, the RSO from bulb #1 is used for ETP-663 analysis and the RSO from bulb #4 is used for ETP-655 analysis.

The ETP-654 measurements of the RSO were performed using the wire grid polarizer at four polarization angles (using both bulbs #1 and #4): 0, 45, 90, and 135 degrees. The polarized RSO curves are shown in Figure 2 (normalized to the maximum of the RSO at 90 degrees). The dominant polarization state is roughly 90 degrees. Also, the Wood's anomaly at around 700 nm is not present for the 0 degrees polarization state (Wood's anomaly is highly polarization dependent).

The polarized RSO measurements were fit to a harmonic function at each wavelength, or

$$I(\lambda) = A(\lambda)\cos(2\alpha + \delta(\lambda)) + C(\lambda), \quad (1)$$

where A is the amplitude, C is an offset, α is the polarization angle, and δ is the phase angle. This equation follows from [9], where only the two-cycle harmonic was retained due to limited data. Next, the degree of polarization was determined from the following,

$$DOP(\lambda) = \frac{I_{\max}(\lambda) - I_{\min}(\lambda)}{I_{\max}(\lambda) + I_{\min}(\lambda)} = \frac{A(\lambda)}{C(\lambda)}, \quad (2)$$

and graphed in Figure 3. The degree of polarization increases with wavelength from about 0 at 400 nm to 95 % at 1100 nm. Also, note the bump at around 700 nm is associated with the Wood's anomaly.

3. ETP-663

ETP-663 was conducted in Pre-TV testing with manual control over the ground support equipment [1]. This test used only band M1 as a sender in the vertical slit configuration. The SpMA used bulb #1 for this test.

The dn was processed in the same manner as in [10], and the description will not be repeated here. The 0.3 ND filter transmission (τ) was determined from ETP-635 [11]; the filter transmission used in this work is listed in Table 2.

The polarized crosstalk is evaluated in terms of crosstalk coefficients which relate the sender to the receiver radiance, corrected by the appropriate RSO. First, the received radiance is given by

$$L_{rec}\left(B_{rec}, D_{rec}, S_{rec}, \lambda_{OOB}, \alpha\right) = \frac{dn_{rec}\left(B_{rec}, D_{rec}, S_{rec}, \lambda_{OOB}, \alpha\right)}{gain\left(B_{rec}, D_{rec}, S_{rec}\right)}, \tag{3}$$

where B, D, S, and λ_{OOB} represent band, detector, subsample, and Out of Band (OOB) wavelength, respectively. The gains were determined in RC-02 part 1 [12], corrected for the SIS100 spectral distribution [13]. The sender radiance is determined by

$$L_{snd}\left(B_{snd}, \lambda_{OOB}, \alpha\right) = \frac{1}{\tau}\left\langle \frac{dn_{snd}\left(B_{snd}, D_{snd}, \lambda_{IB}\right)}{gain\left(B_{snd}, D_{snd}\right)} \right\rangle_{D_{snd}} \frac{RSO_{spma-p}\left(\lambda_{OOB}, \alpha\right)}{RSO_{spma-p}\left(\lambda_{IB}, \alpha\right)} \frac{BW_{VIIRS}(B)}{BW_{SpMA}}. \tag{4}$$

where the average is over all detectors in the sender band and λ_{IB} represents the specified center wavelength for a particular band. BW_{VIIRS} and BW_{SpMA} are the bandwidths of VIIRS bands and the SpMA, respectively (in this work, BW_{SpMA} = 5.5 nm is used) [14]. This equation converts the radiance reaching the sender for an In Band (IB) measurement to the radiance at the desired OOB wavelength. Lastly, the crosstalk coefficient is the ratio of the receiver to the sender radiance, or

$$IC\left(B_{snd}, B_{rec}, D_{rec}, S_{rec}, \lambda_{OOB}, \alpha\right) = \frac{L_{rec}\left(B_{rec}, D_{rec}, S_{rec}, \lambda_{OOB}, \alpha\right)}{L_{snd}\left(B_{snd}, \lambda_{OOB}, \alpha\right)}. \tag{5}$$

For the purposes of this work, the major crosstalk signals have an IC of about 10^{-4} or more.

4. ETP-655

ETP-655 was conducted in TV testing with automatic control over the ground support equipment [2]. Four bands were used as senders (M1, M3, M4, and M6); both the vertical slit and cross slit configurations were used. The SpMA used bulbs #3 (M1 and M4) and bulb #4 (M3 and M6); however, the SpMA RSO was measured for bulb #4, but not bulb #3. In this work, bulb #4 RSO is also used for measurements conducted with bulb #3.

The dn was processed in the same manner as in [10], and will not be repeated here. The ND filter transmissions (τ) were determined from FP-16 data [8]; the filter transmissions used in this work are listed in Table 2.

The polarized crosstalk is evaluated in the same manner as for ETP-663, with the following modification. The sender radiance is now determined by

$$L_{snd}\left(B_{snd},\lambda_{OOB},\alpha\right)=\frac{1}{\tau}\left\langle\frac{dn_{snd}\left(B_{snd},D_{snd},\lambda_{IB}\right)}{gain\left(B_{snd},D_{snd}\right)}\right\rangle_{D_{snd}}\frac{RSO_{spma-p}\left(\lambda_{OOB},\alpha\right)}{RSO_{spma}\left(\lambda_{IB}\right)}\frac{BW_{VIIRS}\left(B\right)}{BW_{SpMA}}. \quad (6)$$

This equation converts the radiance reaching the sender for an IB partially polarized measurement to a radiance at the desired OOB wavelength composed only of light polarized at the desired angle (no IB polarized measurement was made for ETP-655). Here RSO_{spma} and $RSO_{spma\text{-}p}$ represent the partially polarized and polarized RSO, respectively. For the purposes of this work, the major crosstalk signals have an IC of about 10^{-4} or more.

5. Analysis Results

5.1 ETP-663 Results

The dn for detector 9 is graphed versus band in Figure 4 for all six measured wavelengths. The four plots show the response at each of the four measured WGP angles. There is some non-negligible response in M2 at 679 nm. In Figures 5 and 6, the dn for detector 9 is graphed versus band for all four measured WGP angles. Here the six plots correspond to the six measured wavelengths. Again, the dominant OOB feature is at 679 nm in M2, where the 90 degree polarization angle generates the greatest response (which is consistent with Figure 3). In addition, there is some smaller OOB response into M2 at 931 nm and into M3 and M4 at 679 nm. IB response accounts for the signals into M5 at 663 and 679 nm as well as into M7 at 879 nm.

Figure 7 shows IC for M1 and M2 at 679 nm versus detector for all four polarization angles. M1 is the sender band, so the signal is the result of OOB filter leaks; for M2 (which is not directly illuminated), the signal results from wide angle scattering of OOB light below the filter assembly. The middle detectors have higher ICs due to uneven illumination in the track direction [4]. The IC for M1 at 679 nm is largest for the 0 degree polarization angle and smallest for the 90 degree angle. In contrast, the IC for M2 at 679 nm is largest for the 90 degree angle and smallest for the 0 degree angle. The IC for all other bands, wavelengths, and polarization angles is below about 10^{-4}.

5.2 ETP-655 Results

The detector 9 dn is graphed versus band in Figure 8 for all six measured wavelengths (vertical slit on M1). The four plots show the response at each of the four measured WGP angles. Figures 9 and 10 show the dn for detector 9 plotted versus band for all four measured WGP angles. Here the six plots correspond to the six measured wavelengths. There is some non-negligible signal into M2 – M4 at 676 nm, M2 at 803 nm, and M5 at 662 and 676 nm (these wavelengths are IB for M5).

Figure 11 shows the IC for M1 for all six measured OOB wavelengths (vertical slit on M1). The dominant polarization angle for the OOB M1 coefficients is generally 0 or 45 degrees. Figure 12 plots the IC for all six measured wavelengths for receiver band M2 (vertical slit on M2). The crosstalk is small (on the order of 10^{-4} or less) except at wavelengths 676 and 803 nm. At 676 nm, the 90 degree polarization angle is preferred, while at 803 nm, the dominant angles are 45 and 90 degrees. Note that the shape of the profile in the track direction follows the IB profile for 676 and 803 nm, but does not for the other four wavelengths. All other coefficients are below 10^{-4}.

Note that the vertical slit configuration on M1 was measured in both ETP-663 and ETP-655. Following the ETP-663 measurement, it was determined that STR-443 data had under-sampled the tall poles in the OOB; as a result, the tall poles were re-selected using data taken by V. Murgai [7]. A comparison of the results for wavelengths 679 nm (ETP-663) and 676 nm (ETP-655) indicates that the earlier measurement had missed the tall pole (see Figures 7, 11, and 12).

For ETP-655, measurements with the cross-slit were also made; Figures 13 – 15 show the IC from cross-slit measurements on detectors 9, 4, and 14, respectively (676 nm and M1 illuminated). The spike in M1 is clearly centered on the illuminated detector; however, the peak in IC for band M2 – M4 is slightly decreasing in detector number as the distance from the illuminated detector increases. For instance, when the cross-slit is on M1 detector 9, the following is observed in neighboring bands: the peak IC for M2 is still at detector 9 but weighted more heavily to detector 10, the peak IC for M4 is at detector 10, and the peak IC for M3 is at detector 11. This is true for 676 nm when the cross-slit is on detectors 4 and 14 as well and is consistent with the focal plane order of these bands. However, the lower signal at other wavelengths makes it difficult to extrapolate this behavior to other wavelengths.

The plots in Figures 16 and 17 show the dn at detector 9 versus band (vertical slit on M3). Figure 16 graphs all four measured wavelengths for each polarization angle, and Figure 17 graphs all four measured polarization angles for each wavelength. The signal in I1 and M5 at 661 and 676 nm is within the bandpass for both bands. In addition, non-negligible response is observed in M2 and M4 at 676 nm.

Figure 18 plots the IC for M2 – M4 at 676 nm (vertical slit on M3). For M3, the dominant polarization state is 0 degrees, but for M2 and M4, the preferred polarization angle is 90 degrees. All coefficients are below 10^{-4}, except for the case of IB wavelengths for M5. Cross-slit measurements were made for M3 at detector 9 only; results are consistent with the vertical slit measurements.

The dn at detector 9 is graphed versus band in Figures 19 and 20 (vertical slit on M4). Figure 19 graphs all four measured wavelengths for each polarization angle, and Figure 20 graphs all four measured polarization angles for each wavelength. At 607 nm, non-negligible response is observed in bands M2 and M3.

The IC for bands M1 – M4 is plotted in Figure 21 at 607 nm (vertical slit on M4). For the sender band, 0 degrees is the preferred polarization state; however, 45 and 90 degrees are roughly comparable in both M1 and M2 while 45 degrees is dominant in M4. Also, crosstalk is observed into M2 at 596 nm as well as M3 at 596 and 733 nm; all other coefficients are below 10^{-4}. Figure 22 shows the IC for the cross-slit configuration on detector 9 at 607 nm. Results similar to the vertical slit measurements are observed. In addition, the IC peak for the 0 and 45 degree polarization angles is shifted slightly to lower numbered detectors in bands M1 and M2; in contrast, the peak is shift towards higher numbered detectors for band M3. This is consistent with the focal plane order of these bands. In Figures 23 – 25, a double peak centered on the illuminated detector is observed for each of the cross-slit measurements at 733 nm; this double peak is also observed in M3. This double peak is greatest for 0 degrees, but almost non-existent for 90 degrees.

The plots in Figures 26 and 27 show the dn at detector 9 versus band (vertical slit on M6). Figure 26 graphs all three measured wavelengths for each polarization angle, and Figure 27 graphs all four measured polarization angles for each wavelength. The response in M2 at 448 nm is within the M2 bandpass.

The only IC above the 10^{-4} level observed for sender M6 was into M2 at IB wavelengths. Figure 28 graphs IC for band M6 at all three measured wavelengths (cross-slit on detector 9). Note that for 834 nm, a double peak in the IC is observed centered around detector position 9. This double peak is greatest for 0 degrees, but almost non-existent for 90 degrees.

6. Summary

- The degree of polarization for the SpMA increase from close to 0 at 400 nm to 95% at 1100 nm. The dominant polarization state of the SpMA is close to 90 degrees.
- Major optical crosstalk pathways are observed from:
    - M1 into M2 and M3 at 676 nm;
    - and M4 into M1 at 607 nm, into M2 at 596 and 607 nm, as well as into M3 at 596, 607, and 733 nm.
- Crosstalk is generally largest for above crosstalk pathways at the 90 degree polarization angle. The polarization favored in the scan direction is generally orthogonal to the polarization favored in the track direction.
- Preferred scattering angle slightly off scan direction at 676 nm from M1 and at 607 nm from M4.
- Double peak in track direction centered on the illuminated detector observed for M4 at 733 nm and M6 at 834 nm.

Acknowledgement

The sensor test data used in this document was provided by the Raytheon El Segundo testing team. Approaches for data acquisition and data reductions, as well as data extraction tools were also provided by the Raytheon El Segundo team. We would like to thank the Raytheon El Segundo team for their support. The data analysis tools were developed by the NICST team.

Table 1: ETP-655 and ETP-663 test data

UAID	Sender Band	ND filter	Collects	Slit	Wavelengths	E side	Test
U3103271	M1	0.3	26--29	vertical	412	A	ETP-663
U3103271	M1	~	1--24	vertical	663, 679, 769, 799, 879, 931	A	ETP-663
U3104167	M1	0.4	11	vertical	415	A	ETP-655
U3104172	M1	~	1--30	vertical	624, 645, 662, 676, 787, 803	A	ETP-655
U3104174	M1	0.4	1	detector 9	411	A	ETP-655
U3104175	M1	~	1--30	detector 9	624, 645, 662, 676, 787, 803	A	ETP-655
U3104177	M1	0.4	1	detector 4	411	A	ETP-655
U3104178	M1	~	1--30	detector 4	624, 645, 662, 676, 787, 803	A	ETP-655
U3104180	M1	0.4	1	detector 14	411	A	ETP-655
U3104181	M1	~	1--30	detector 14	624, 645, 662, 676, 787, 803	A	ETP-655
U3104235	M3	0.8	8	vertical	481	B	ETP-655
U3104240	M3	~	1--20	vertical	661, 676, 784, 800	B	ETP-655
U3104241	M3	0.8	2	detector 9	487	B	ETP-655
U3104242	M3	~	1--20	detector 9	661, 676, 784, 800	B	ETP-655
U3104132	M4	1.2	9	vertical	553	A	ETP-655
U3104138	M4	~	1--15	vertical	596, 607, 733	A	ETP-655
U3104140	M4	1.2	1	detector 9	555	A	ETP-655
U3104141	M4	~	1--15	detector 9	596, 607, 733	A	ETP-655
U3104143	M4	1.2	1	detector 4	555	A	ETP-655
U3104144	M4	~	1--15	detector 4	596, 607, 733	A	ETP-655
U3104146	M4	1.2	1	detector 14	555	A	ETP-655
U3104147	M4	~	1--15	detector 14	596, 607, 733	A	ETP-655
U3104269	M6	1.3	9	vertical	744	B	ETP-655
U3104274	M6	~	1--15	vertical	448, 640, 834	B	ETP-655
U3104275	M6	1.3	1	detector 9	745	B	ETP-655
U3104276	M6	~	1 -- 15	detector 9	448, 640, 834	B	ETP-655

Table 2: ND filter transmissions

Band	ND filter	τ
M1	0.3	0.5010
M1	0.4	0.4151
M3	0.8	0.1723
M4	1.2	0.0690
M6	1.3	0.0539

Figure 1: SpMA RSO for bulbs #1 and #4

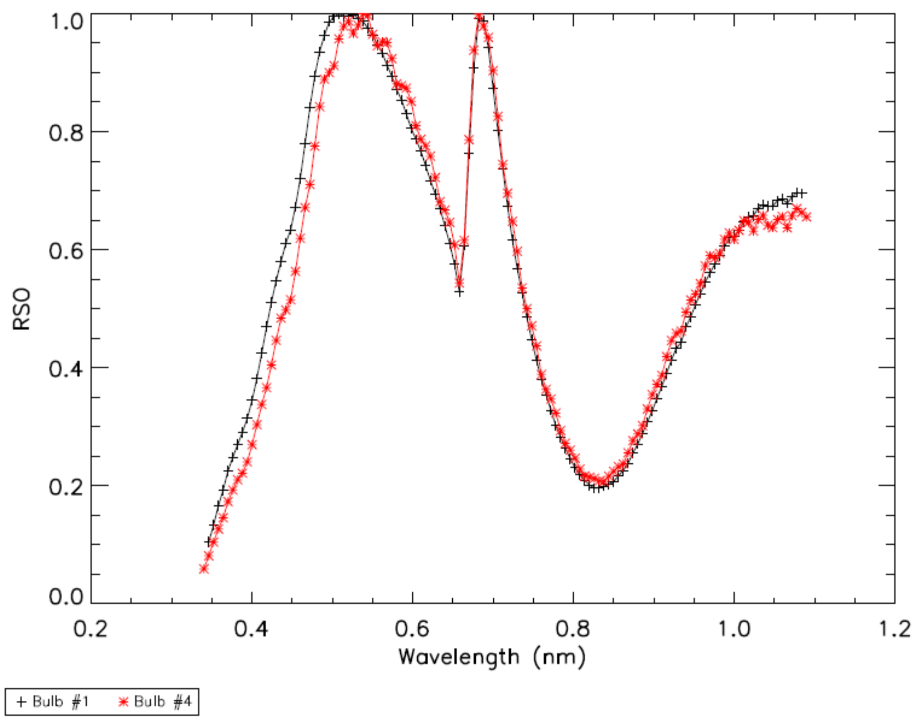

Figure 2: SpMA polarized RSO for bulbs #1 and #4

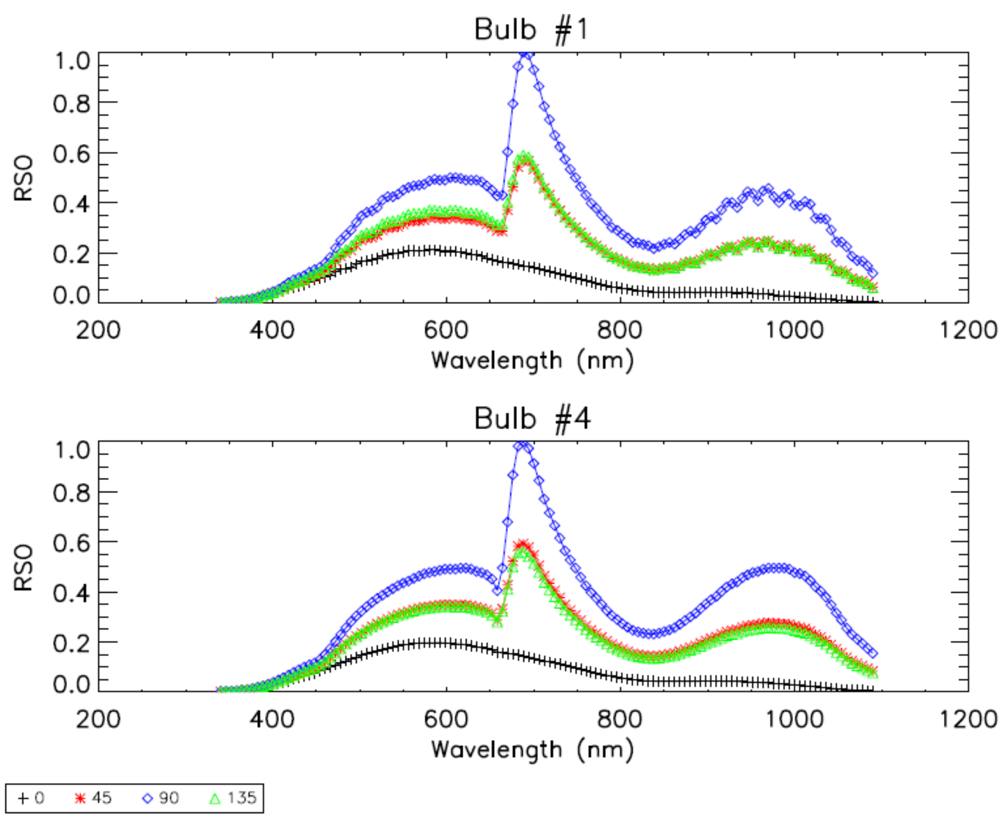

Figure 3: Degree of Polarization for bulbs #1 and #4

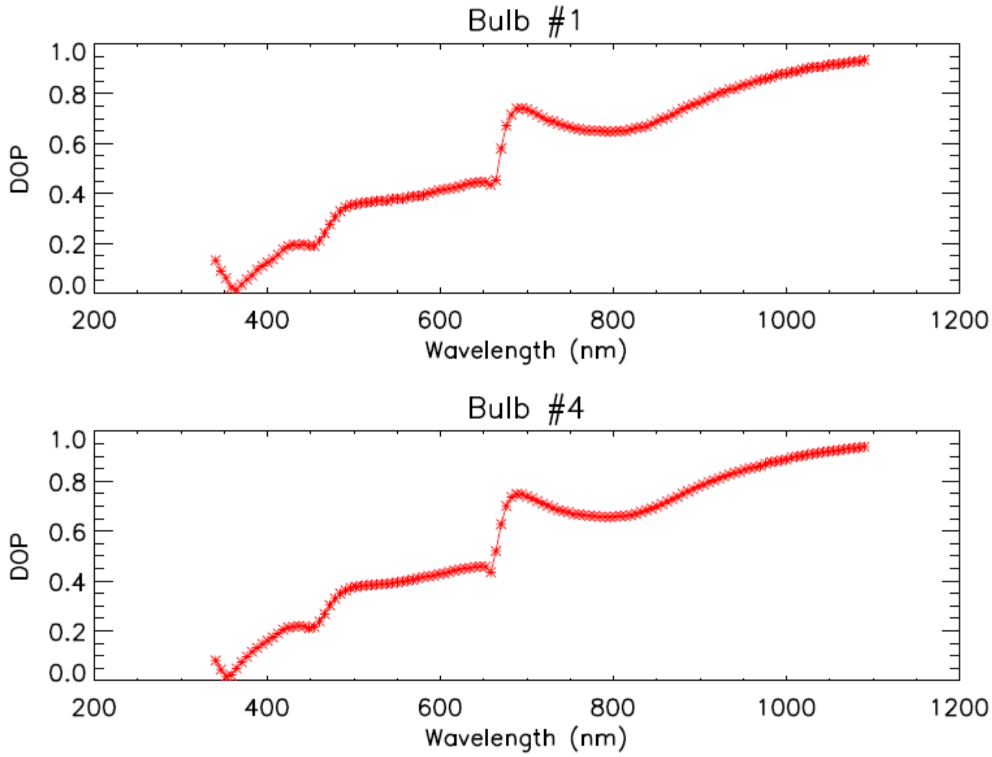

Figure 4: ETP-663 dn versus band for detector 9

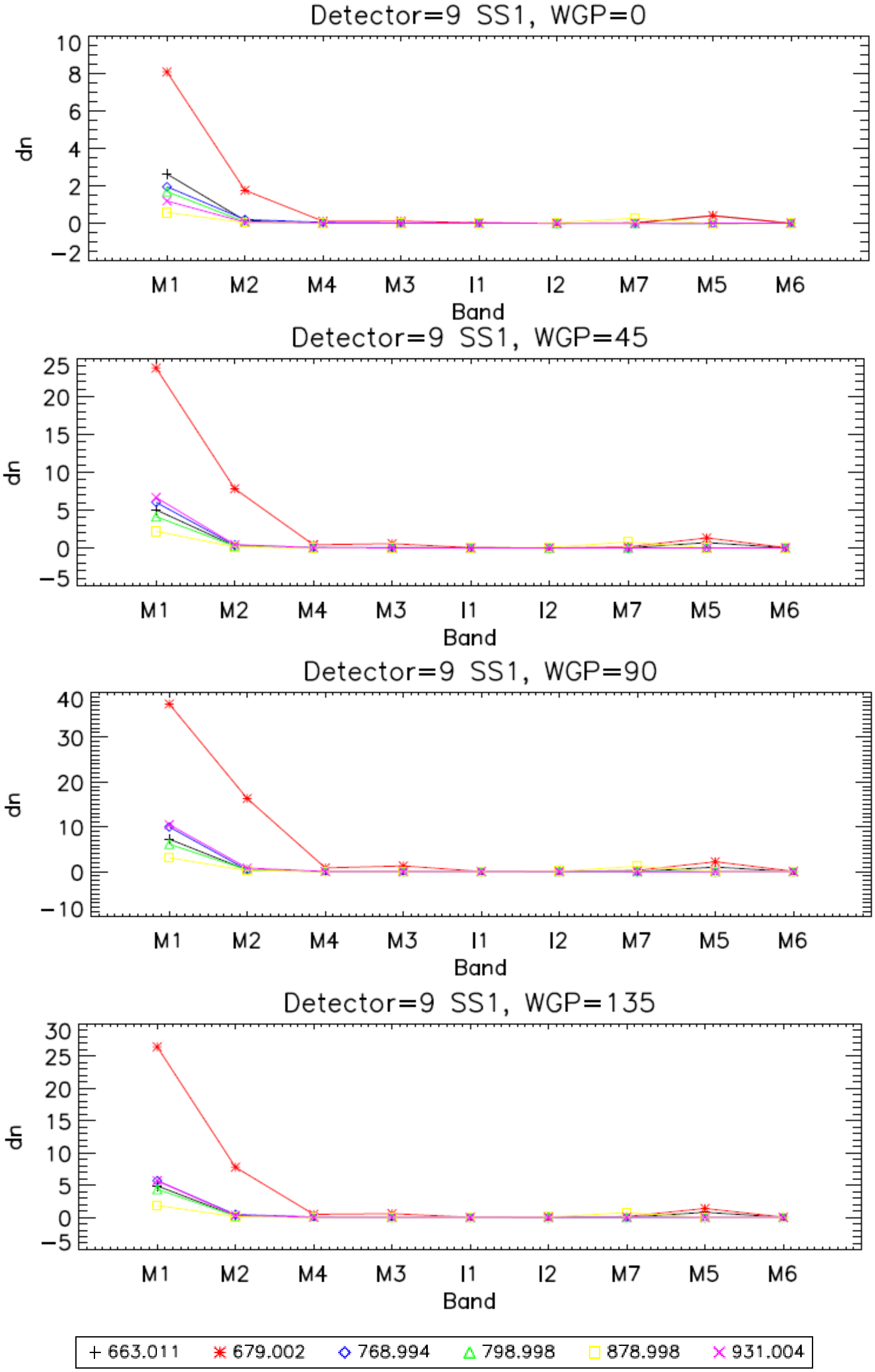

Figure 5: ETP-663 dn versus WGP angle for detector 9

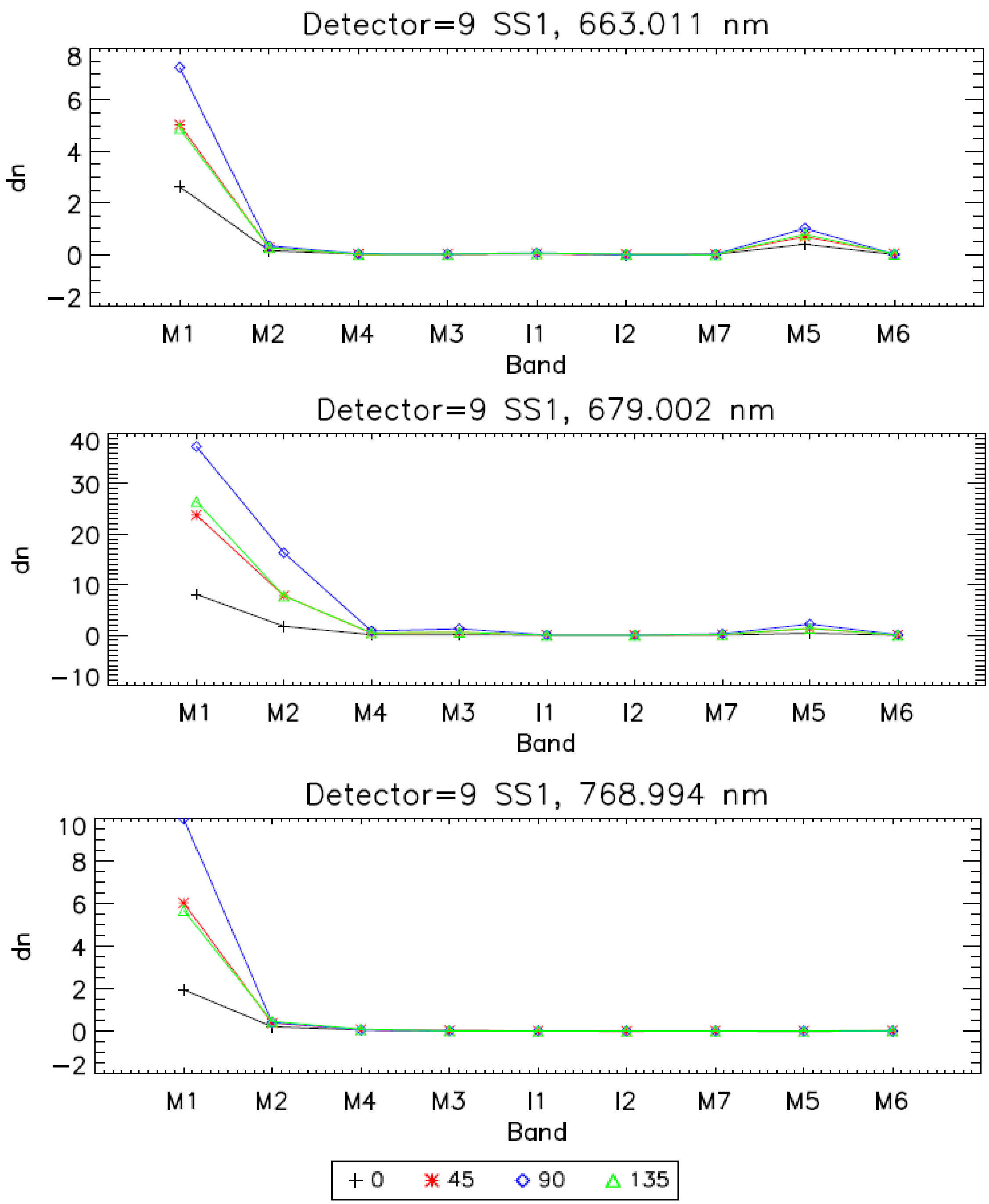

Figure 6: ETP-663 dn versus WGP angle for detector 9

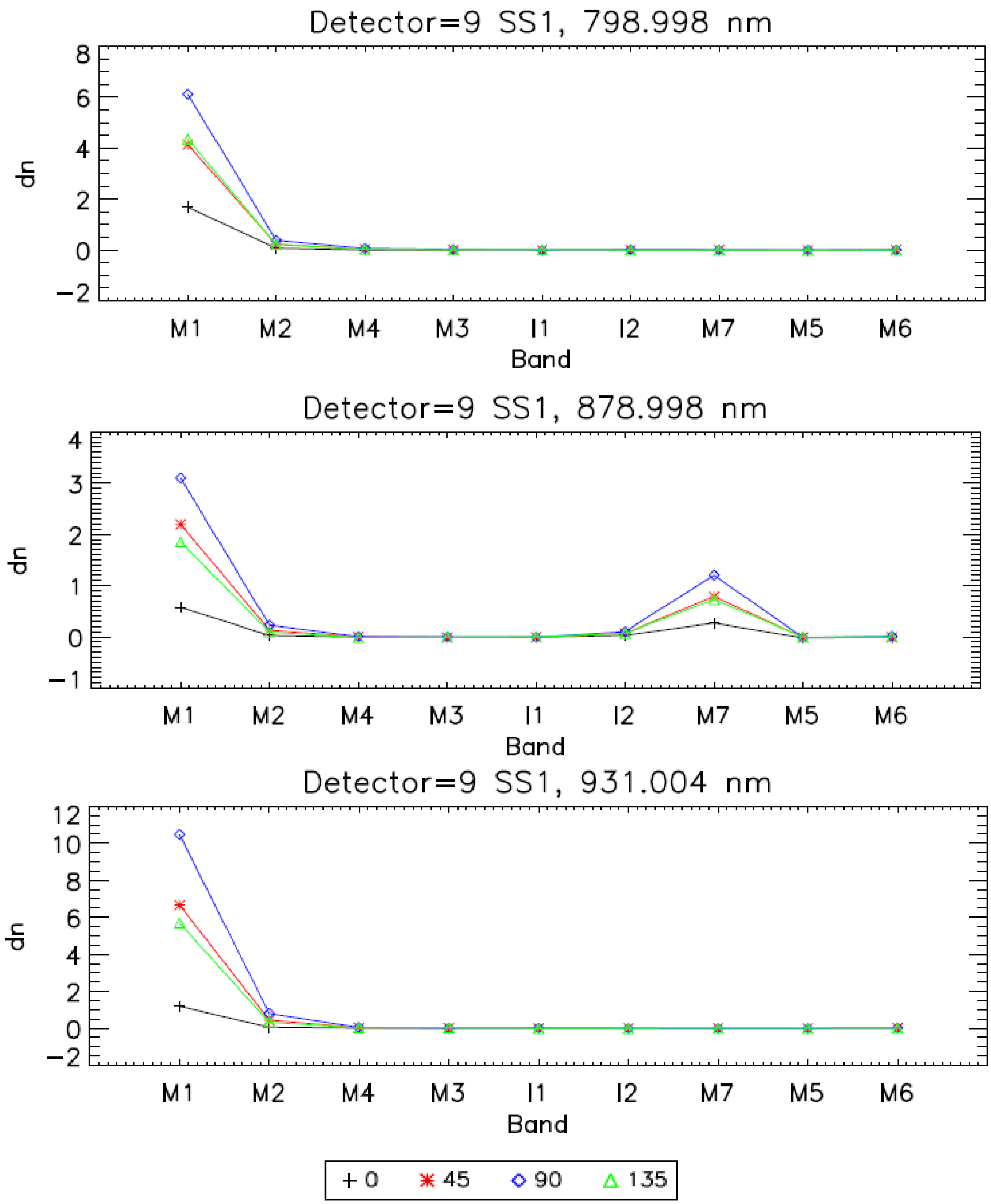

Figure 7: ETP-663 IC for M1 and M2 at 679 nm

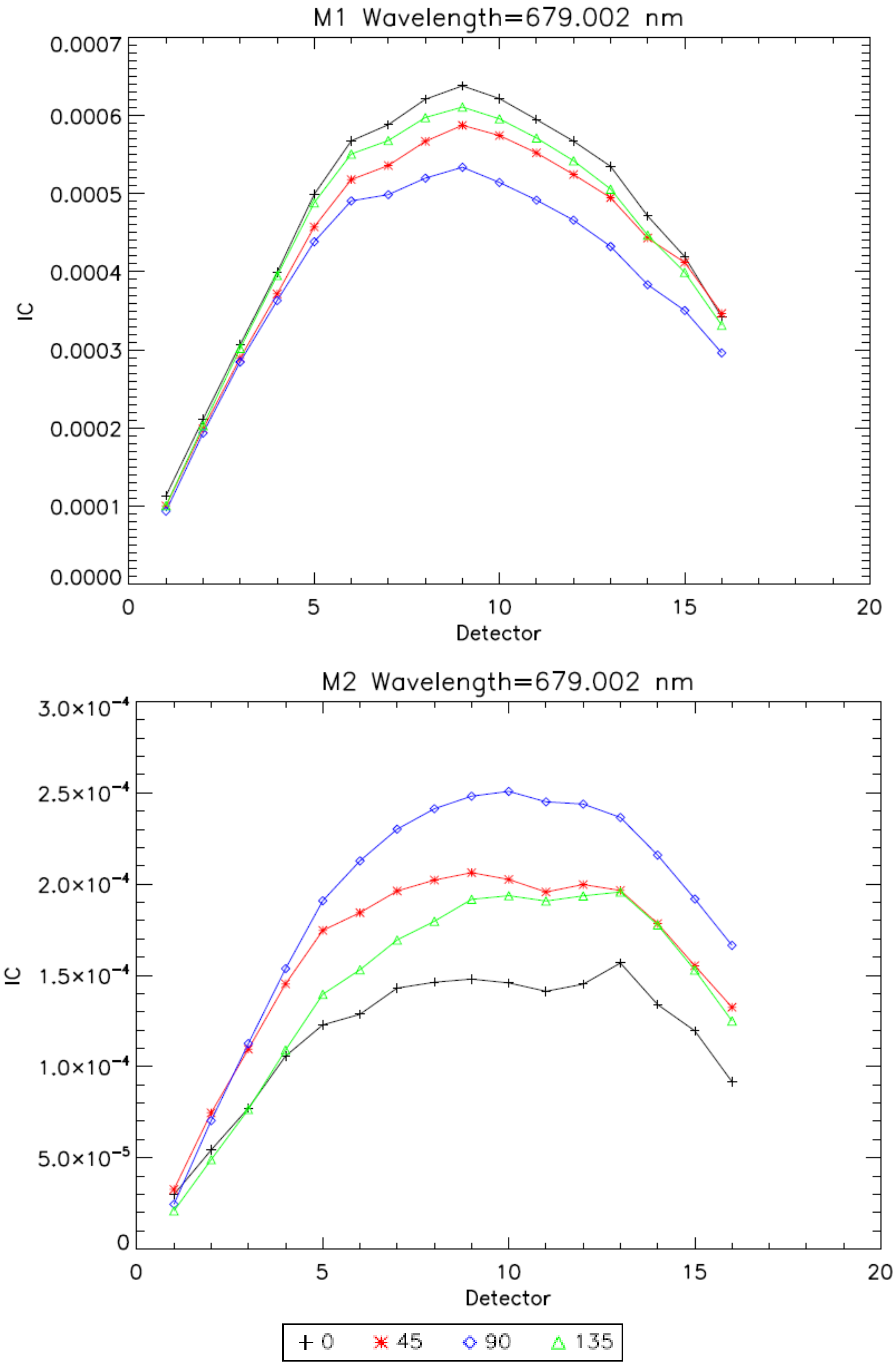

Figure 8: ETP-655 dn versus band for detector 9 (vertical slit on M1)

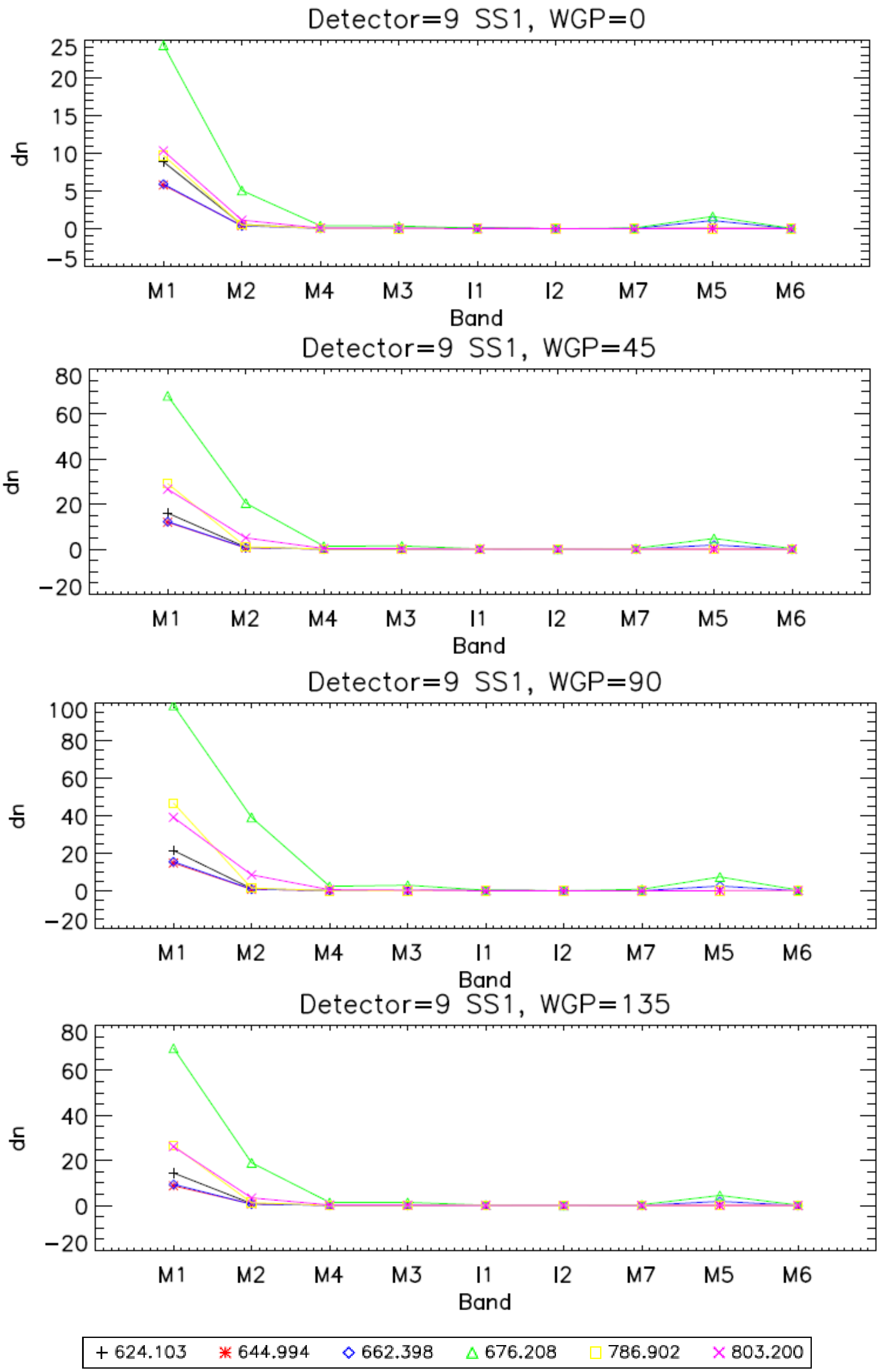

Figure 9: ETP-655 dn versus WGP angle for detector 9 (vertical slit on M1)

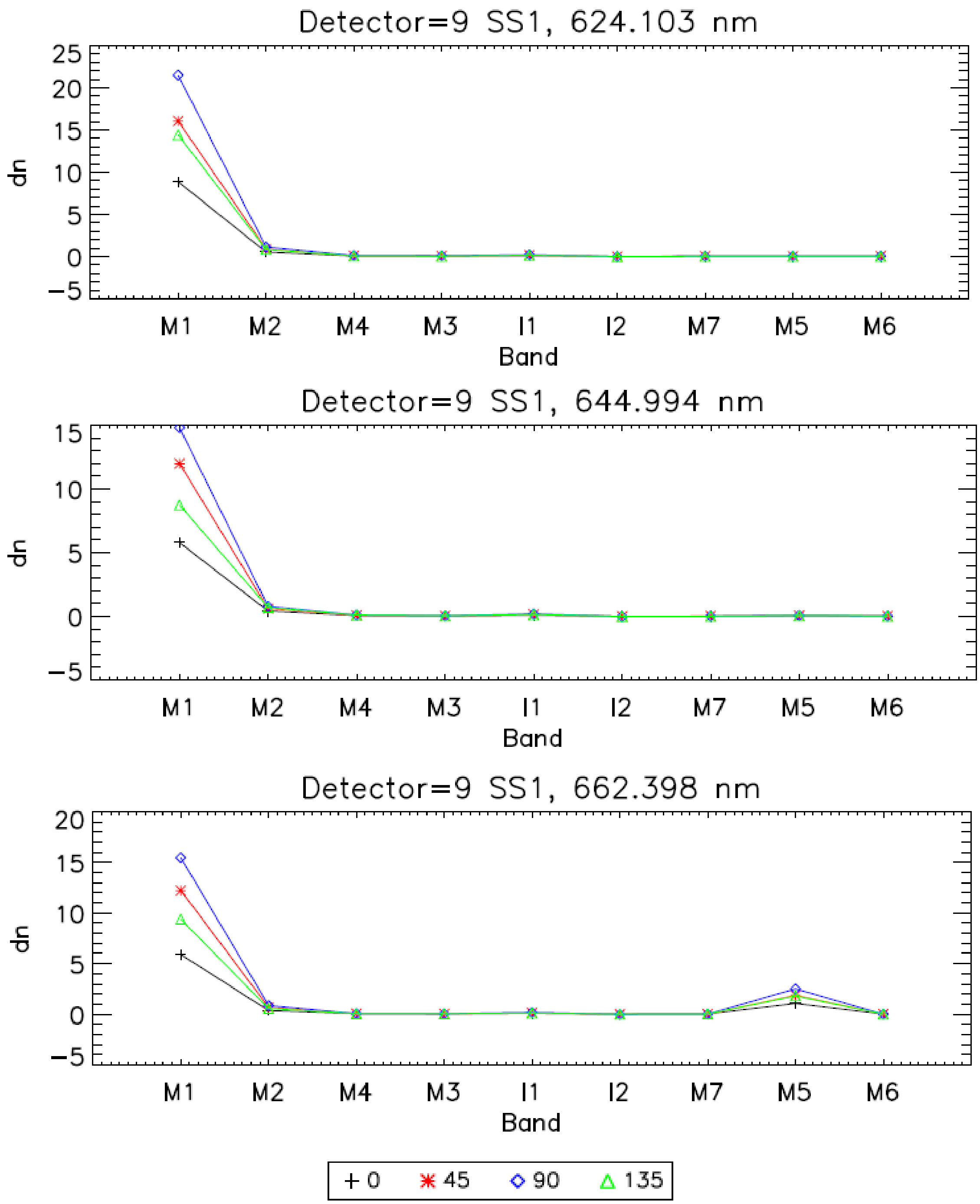

Figure 10: ETP-655 dn versus WGP angle for detector 9 (vertical slit on M1)

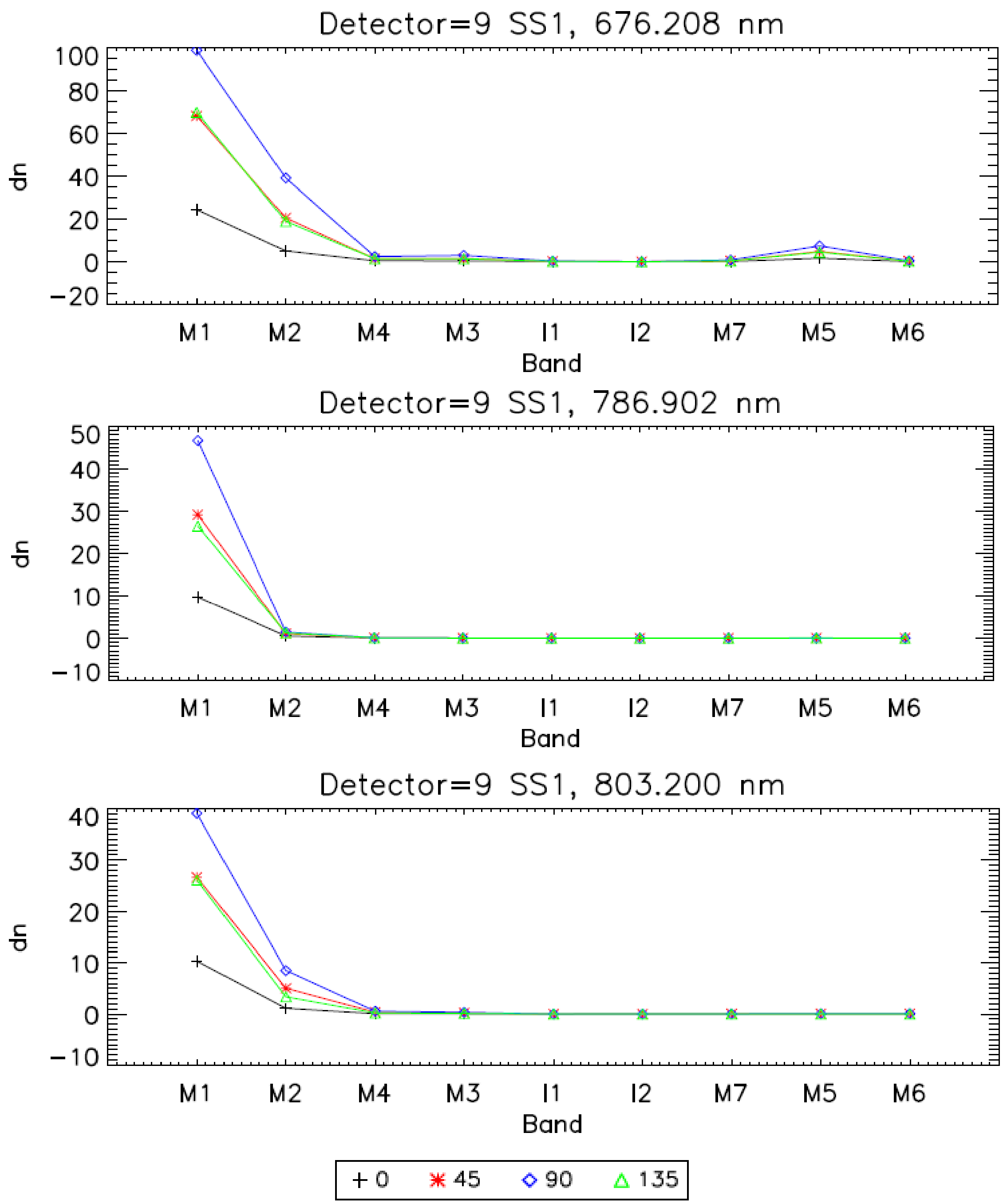

Figure 11: ETP-655 IC for M1 (vertical slit on M1)

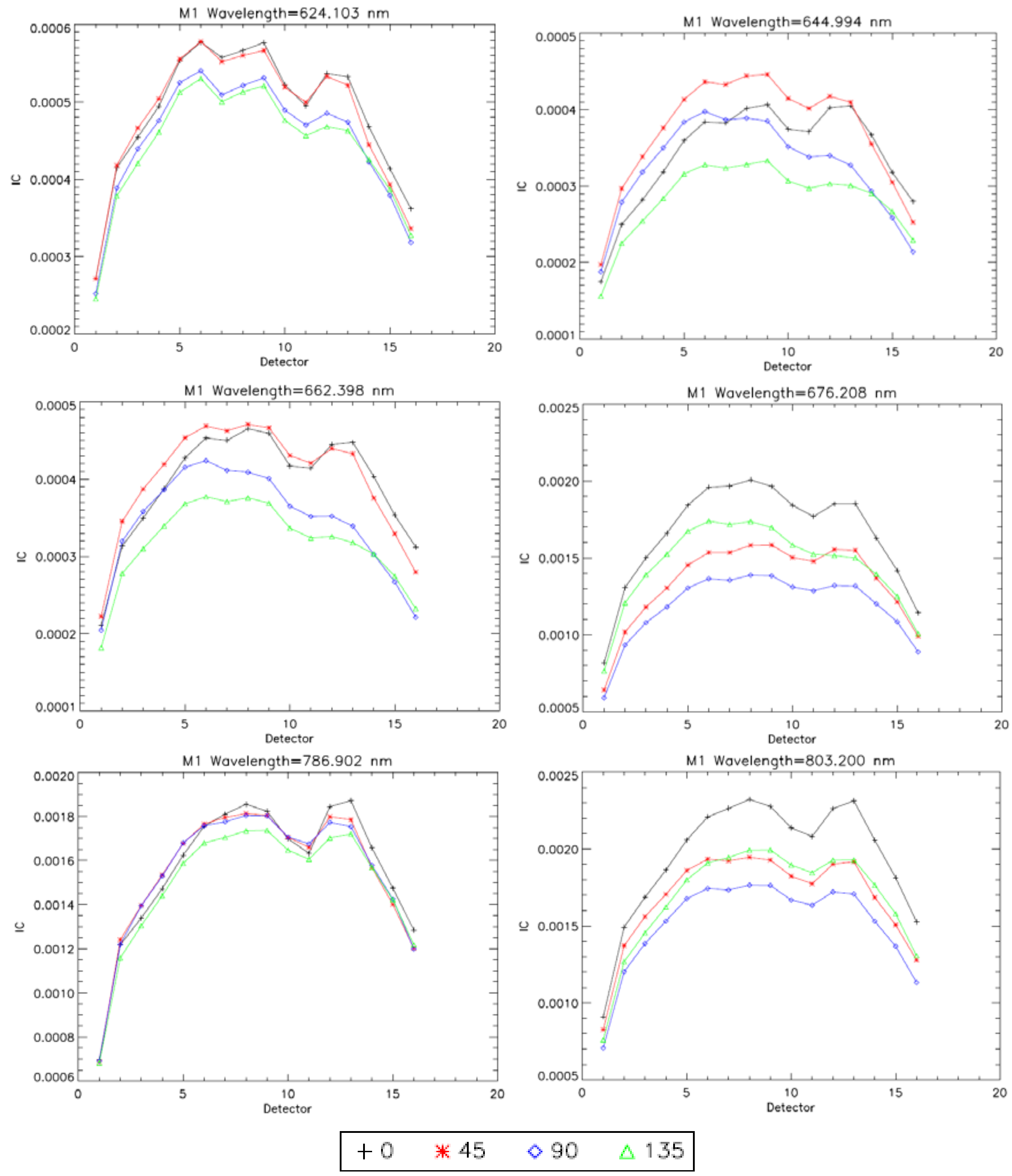

Figure 12: ETP-655 IC for M2 (vertical slit on M1)

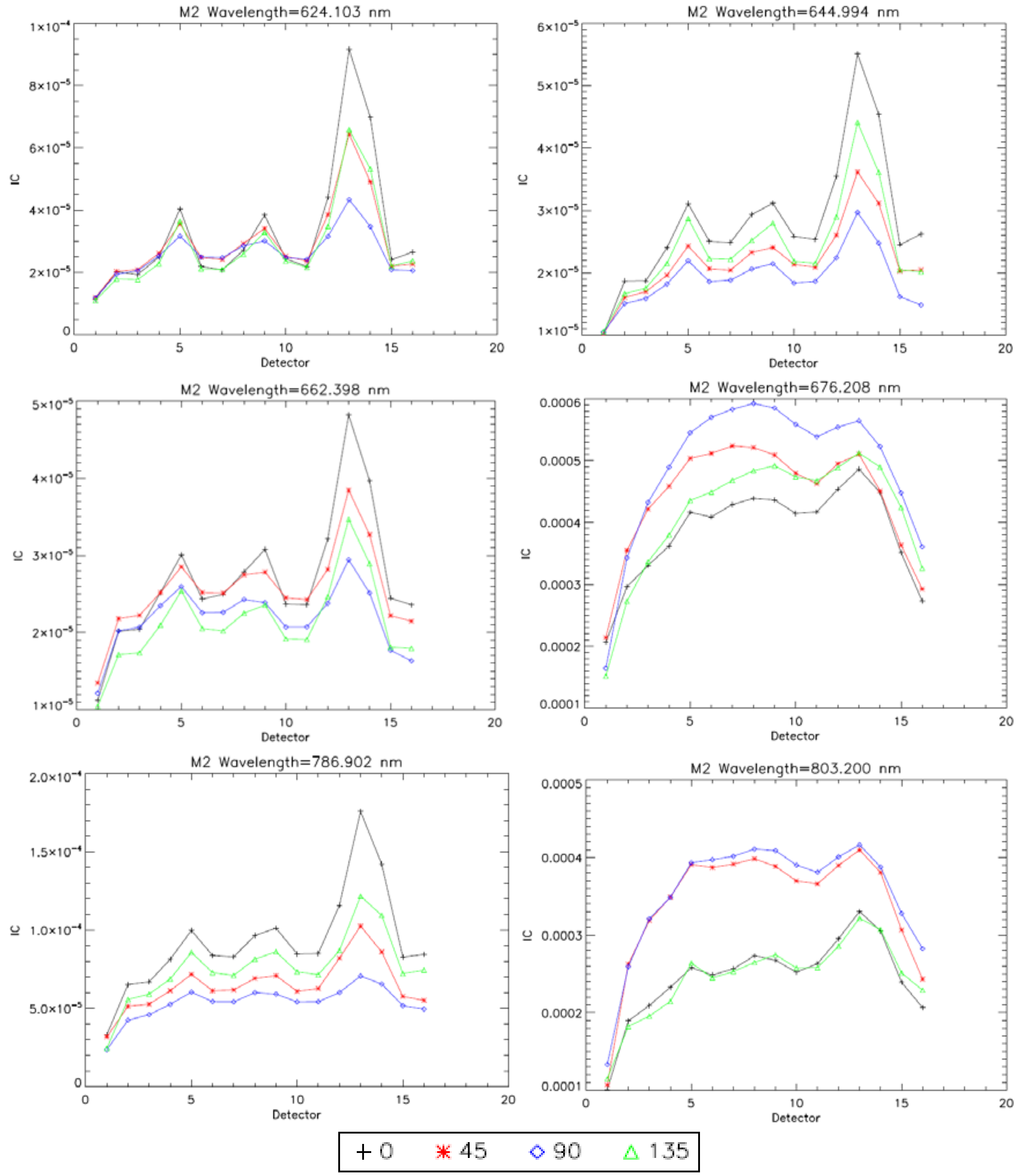

Figure 13: ETP-655 IC for M1-M4 at 676 nm (cross-slit on M1 detector 9)

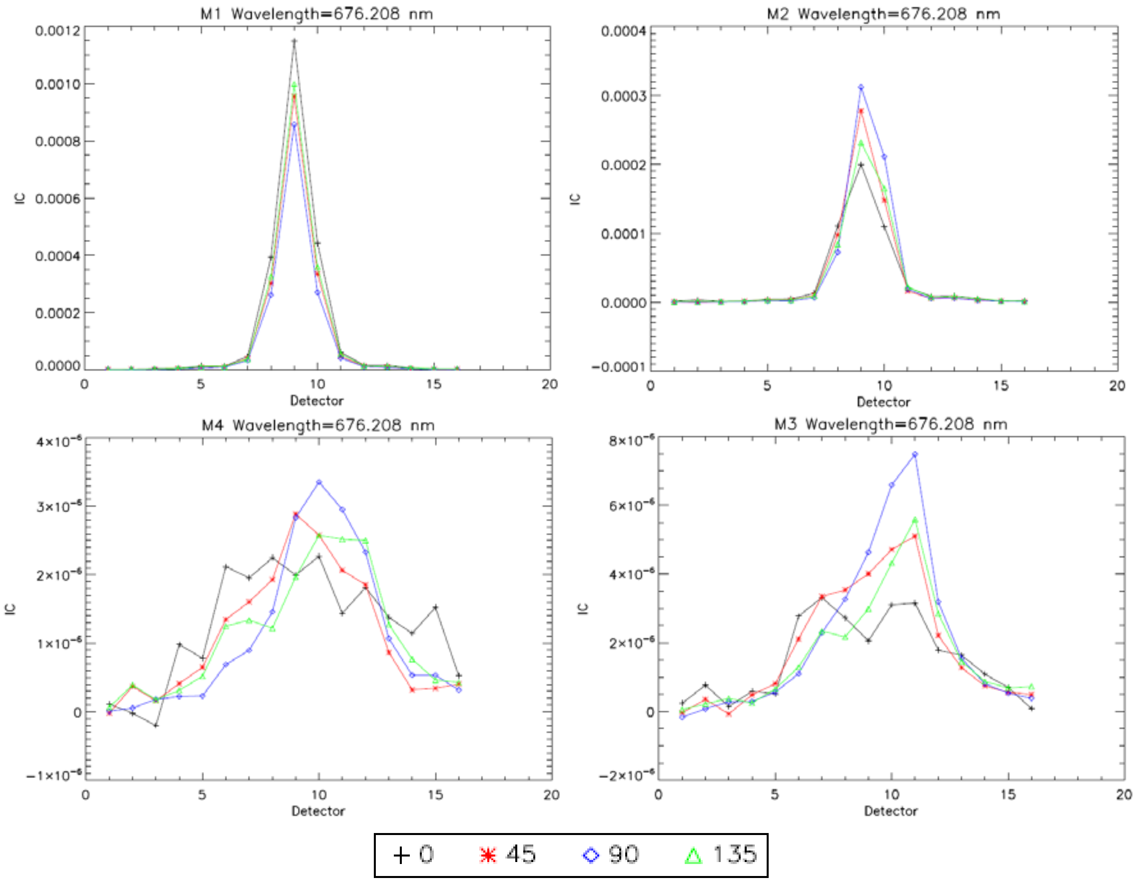

Figure 14: ETP-655 IC for M1-M4 at 676 nm (cross-slit on M1 detector 4)

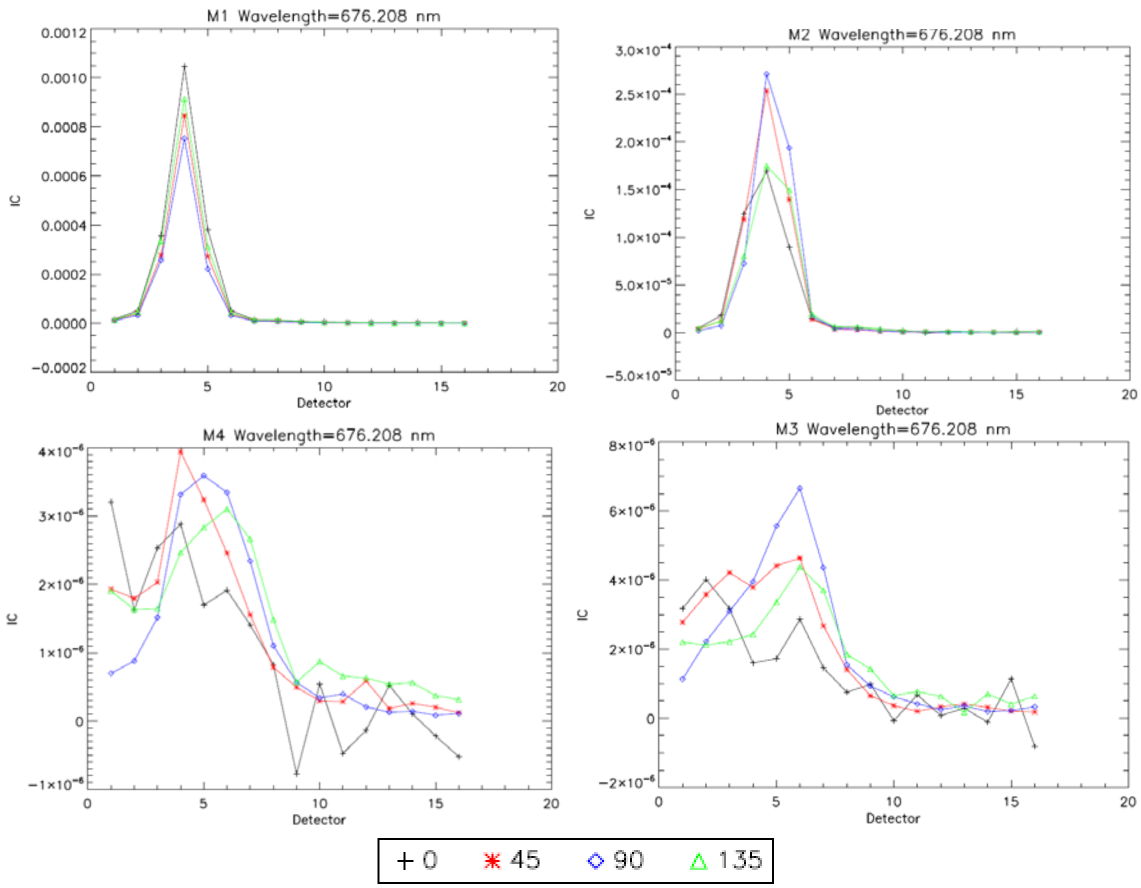

Figure 15: ETP-655 IC for M1-M4 at 676 nm (cross-slit on M1 detector 14)

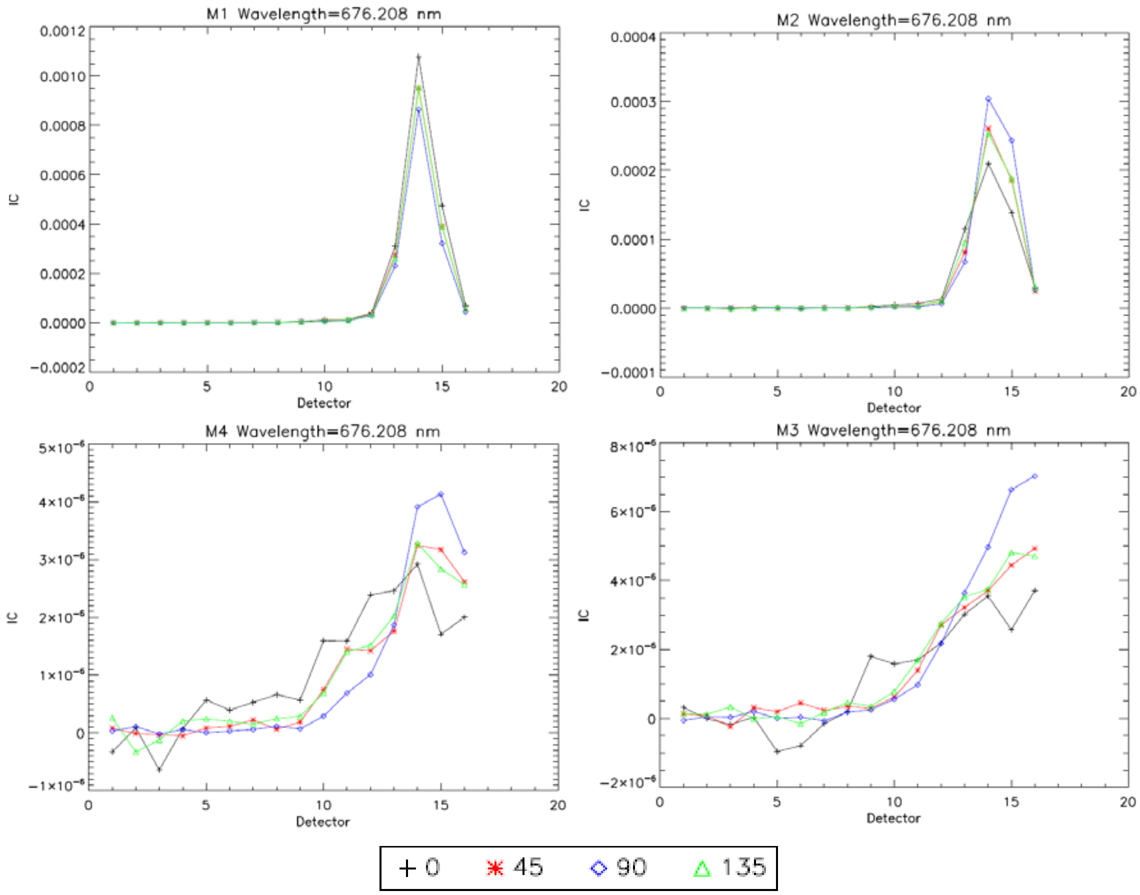

Figure 16: ETP-655 dn versus band for detector 9 (vertical slit on M3)

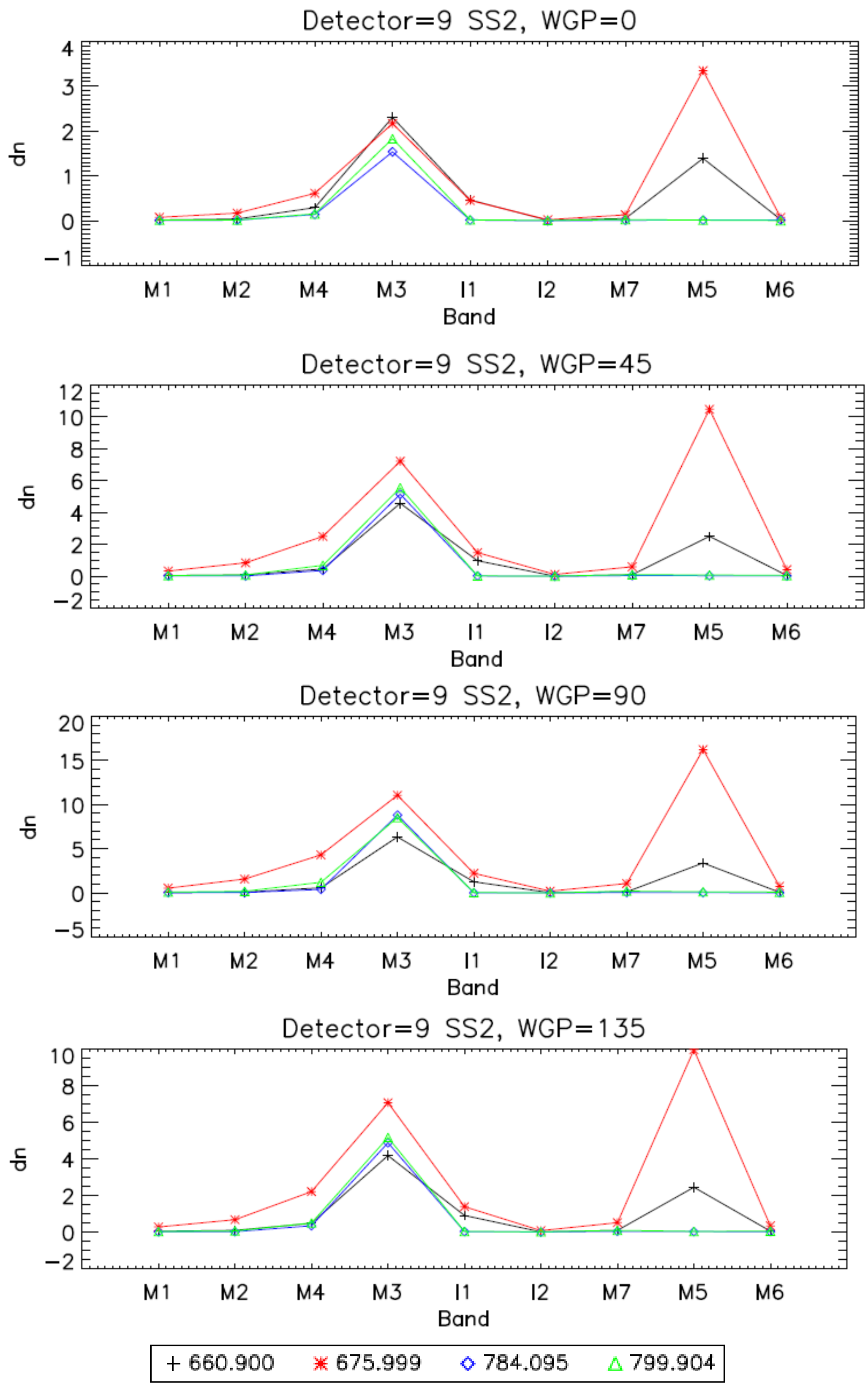

Figure 17: ETP-655 dn versus WGP angle for detector 9 (vertical slit on M3)

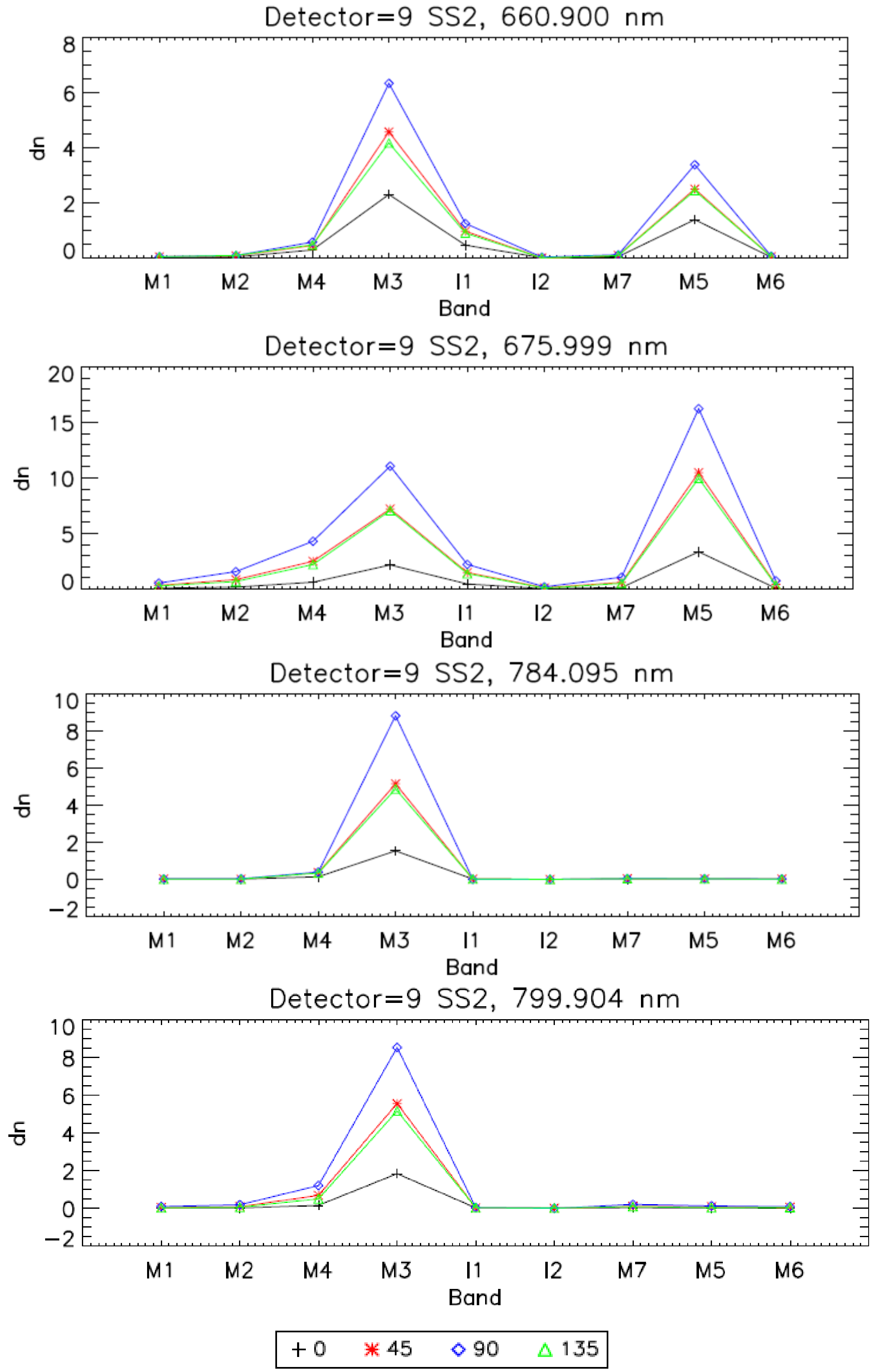

Figure 18: ETP-655 IC for M2-M4 for 676 nm (vertical slit on M3)

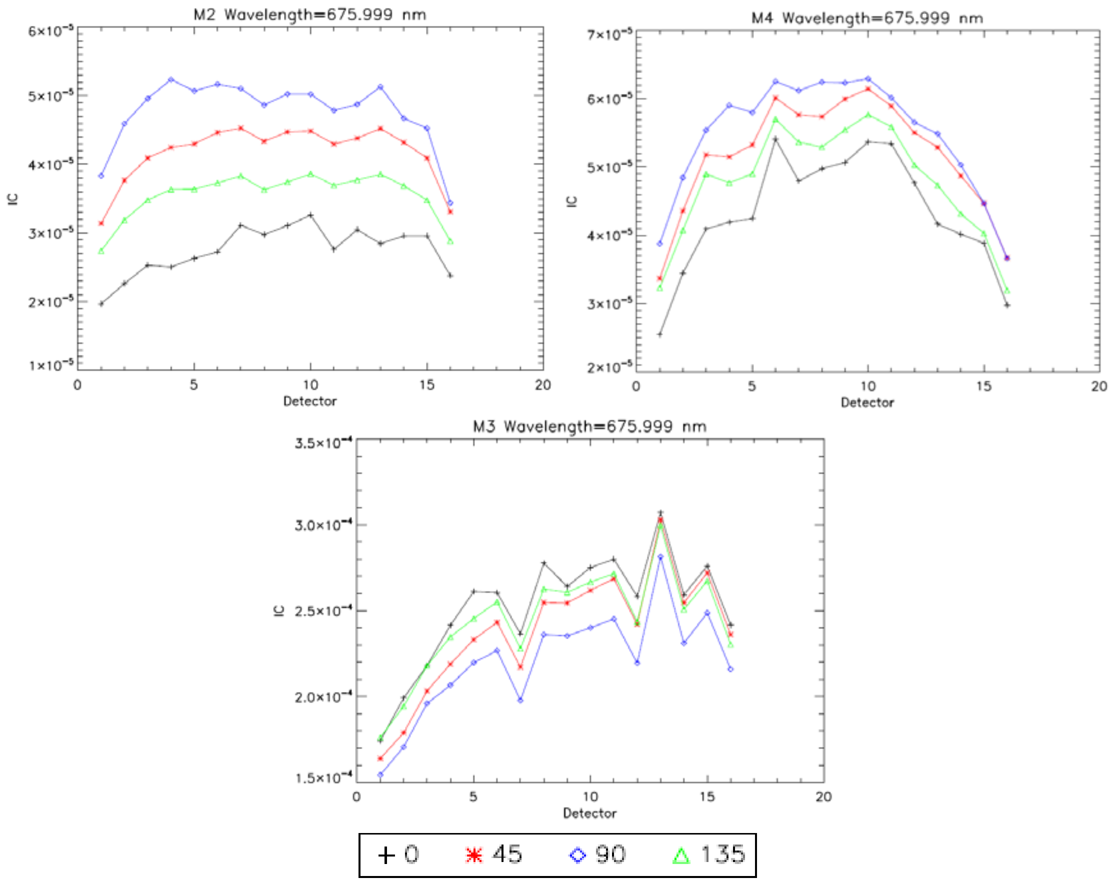

Figure 19: ETP-655 dn versus band for detector 9 (vertical slit on M4)

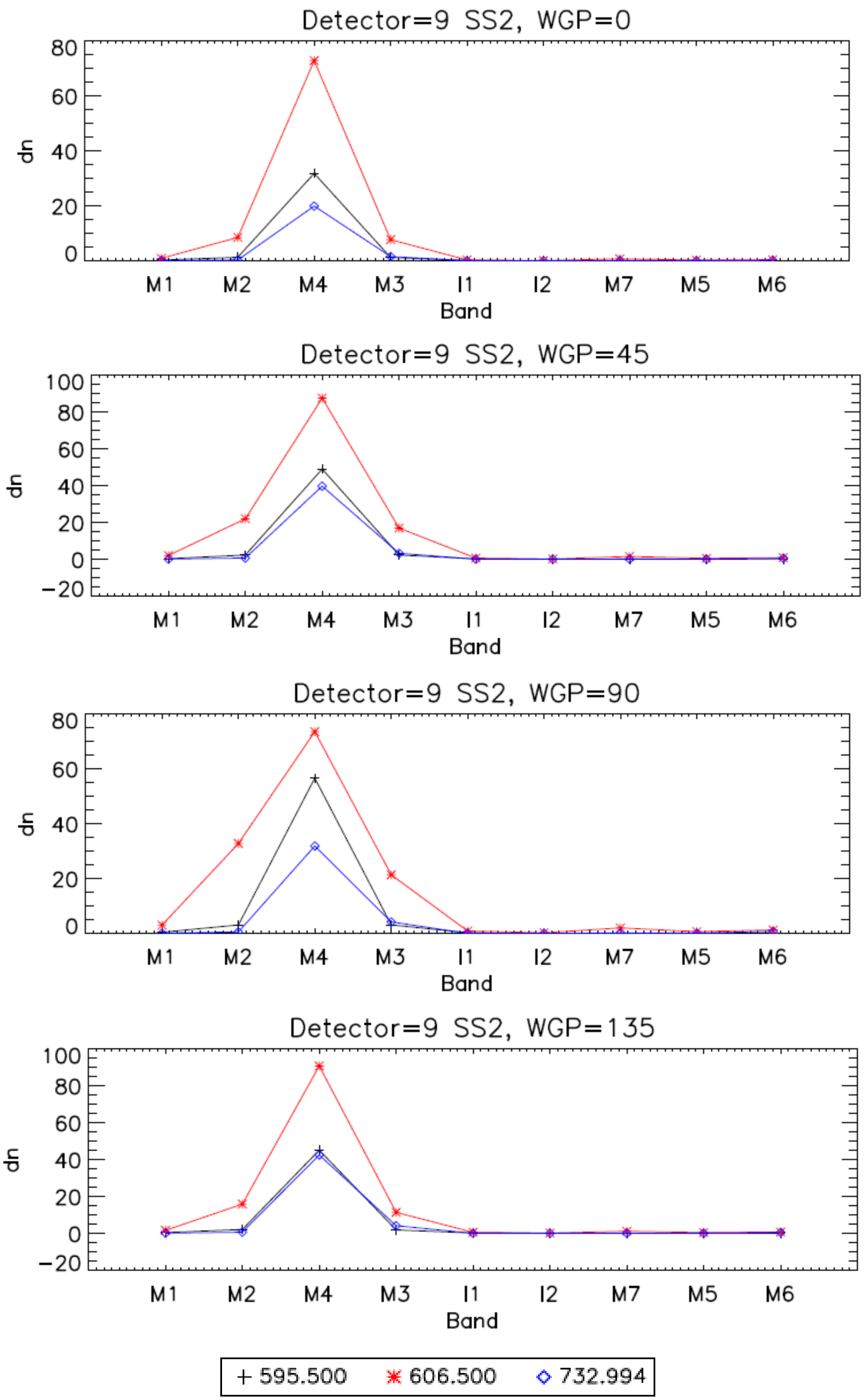

Figure 20: ETP-655 dn versus WGP angle for detector 9 (vertical slit on M4)

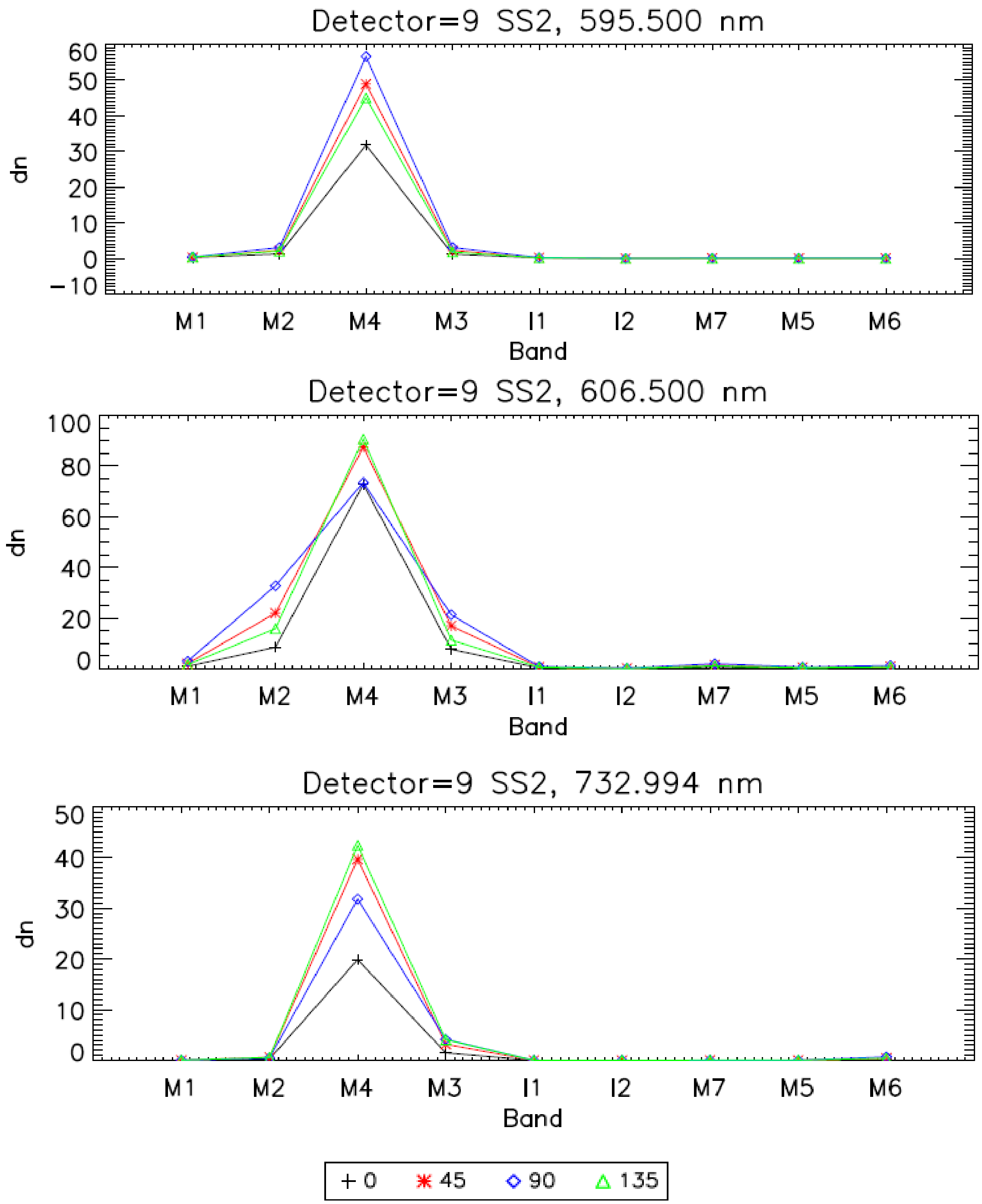

Figure 21: ETP-655 IC for M1-M4 for 607 nm (vertical slit on M4)

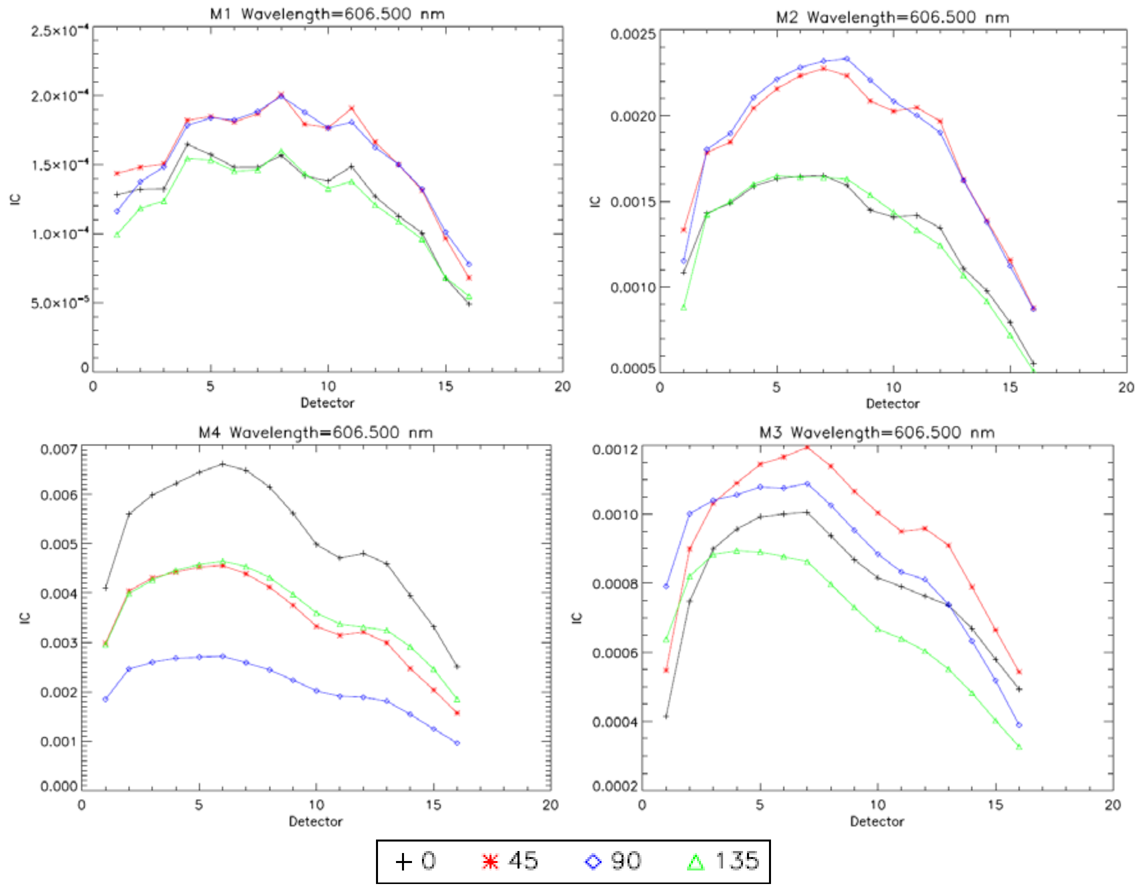

Figure 22: ETP-655 IC for M1-M4 at 606 nm (cross-slit on M4 detector 9)

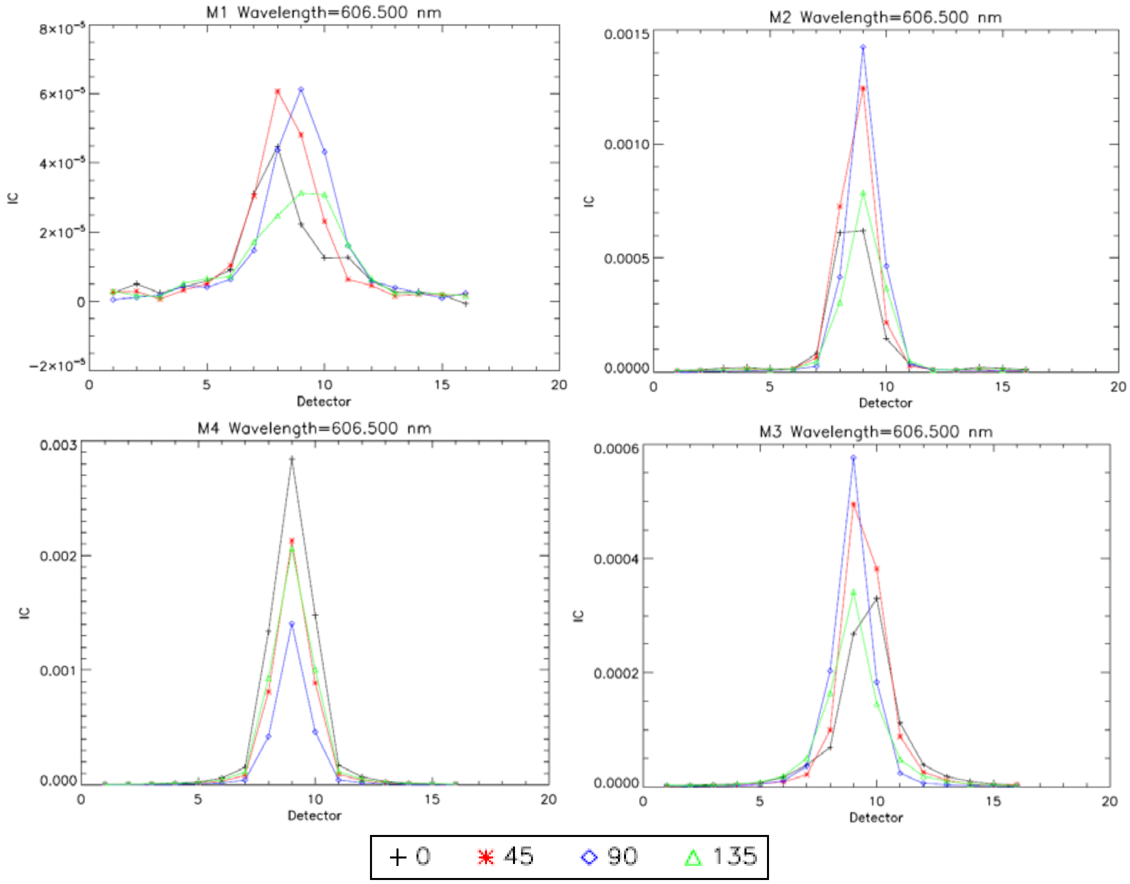

Figure 23: ETP-655 IC for M3-M4 at 732 nm (cross-slit on M4 detector 9)

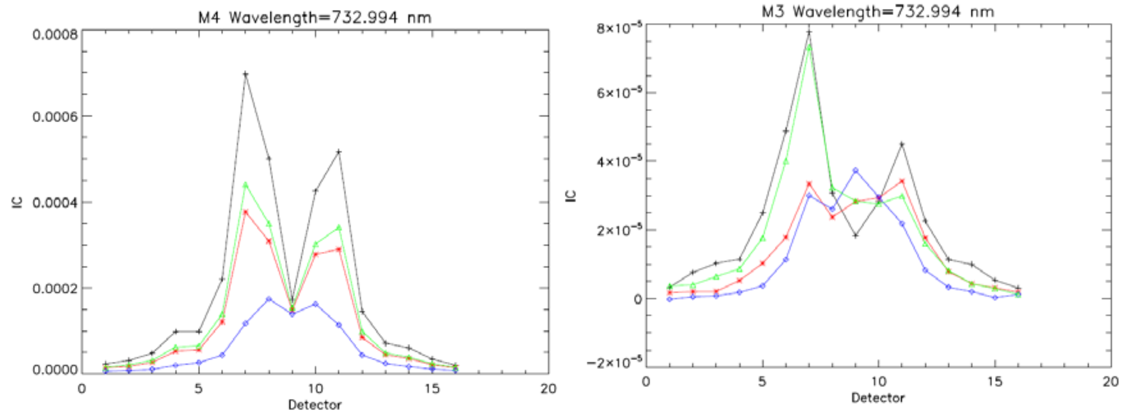

Figure 24: ETP-655 IC for M3-M4 at 732 nm (cross-slit on M4 detector 4)

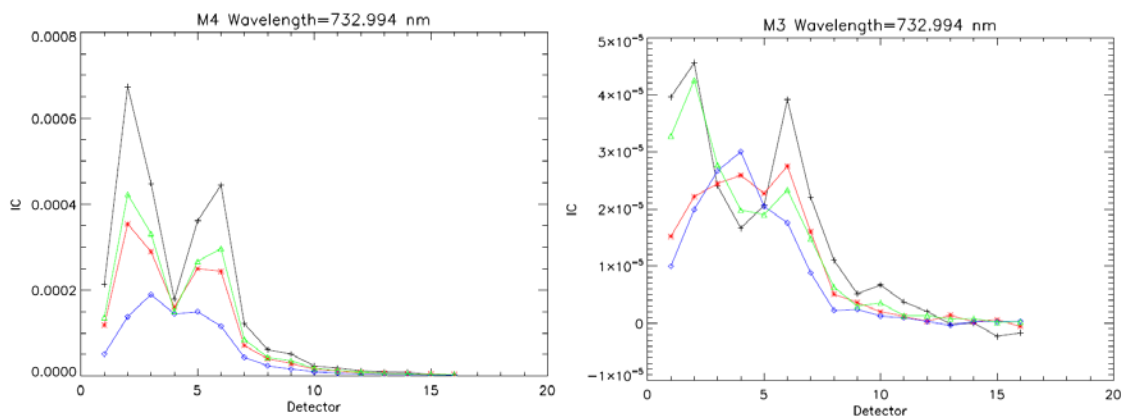

Figure 25: ETP-655 IC for M3-M4 at 732 nm (cross-slit on M4 detector 14)

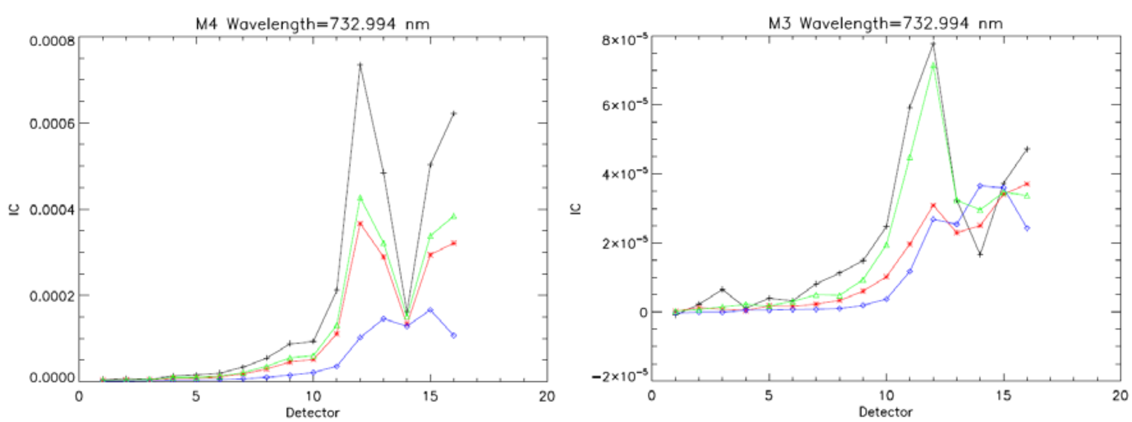

Figure 26: ETP-655 dn versus band for detector 9 (vertical slit on M6)

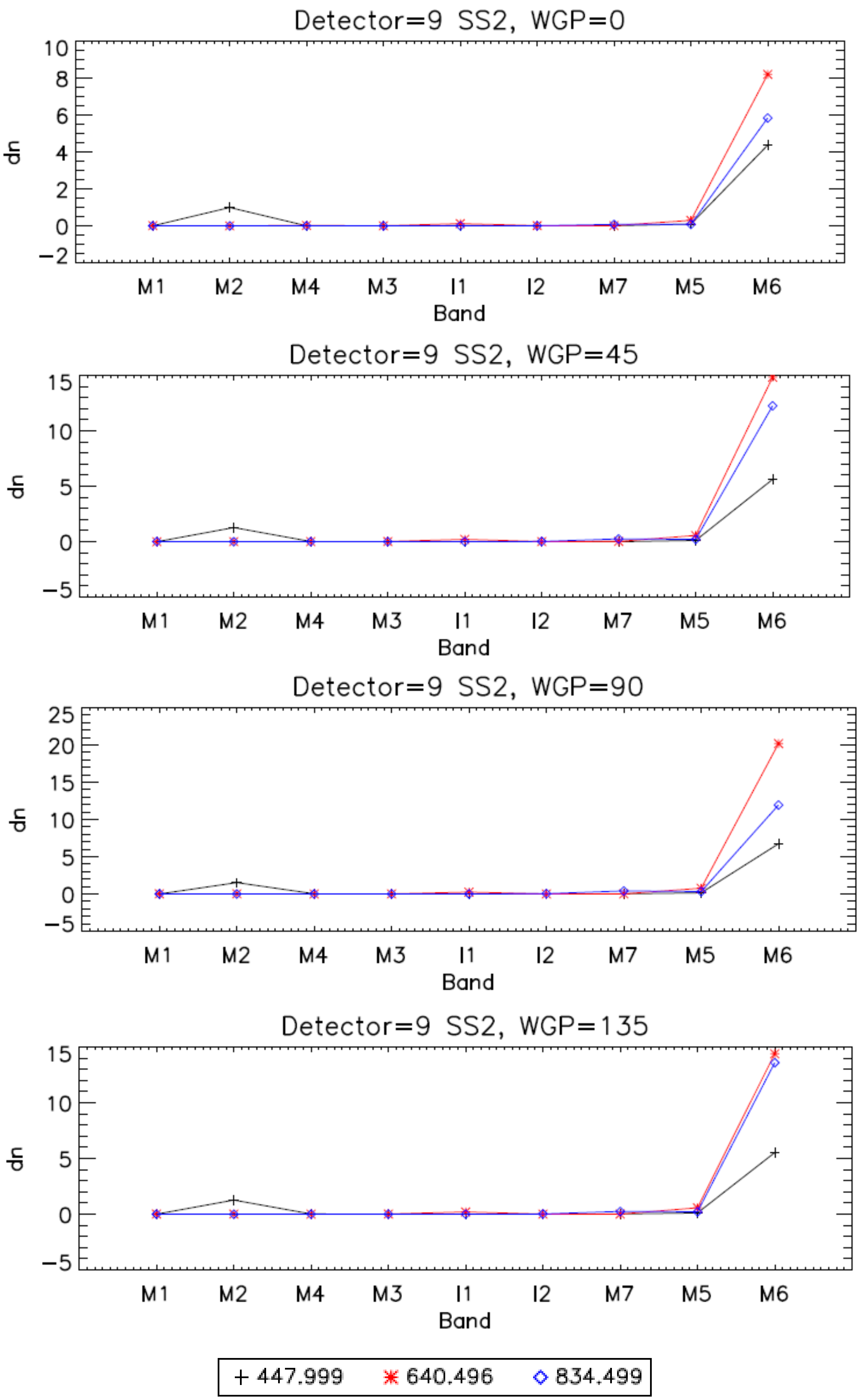

Figure 27: ETP-655 dn versus WGP angle for detector 9 (vertical slit on M6)

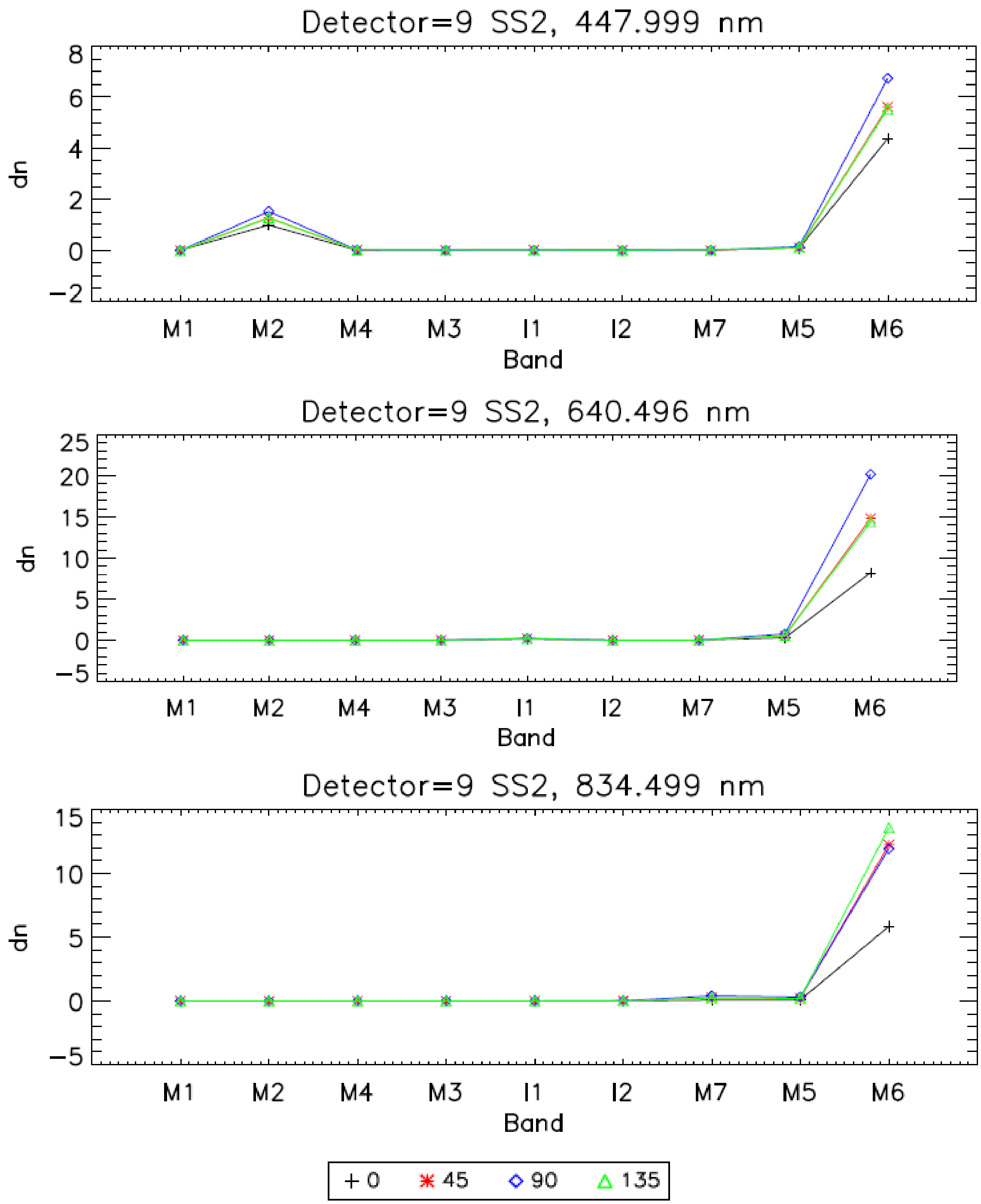

Figure 28: ETP-655 IC for M6 (cross-slit on M6 detector 9)